HHS Public Access

Author manuscript

Dev Biol. Author manuscript; available in PMC 2016 June 15.

Published in final edited form as:

Dev Biol. 2015 June 15; 402(2): 253–262. doi:10.1016/j.ydbio.2015.03.011.

Kif18a is specifically required for mitotic progression during germ line development

Anne Czechanski[1], **Haein Kim**[2], **Candice Byers**[1], **Ian Greenstein**[1], **Jason Stumpff**[#2], and **Laura G. Reinholdt**[#1]

[1]The Jackson Laboratory, Genetic Resource Science, Bar Harbor, ME 04609

[2]Department of Molecular Physiology and Biophysics, University of Vermont, Burlington, VT 05405

[#] These authors contributed equally to this work.

Abstract

Genome integrity in the developing germ line is strictly required for fecundity. In proliferating somatic cells and in germ cells, there are mitotic checkpoint mechanisms that ensure accurate chromosome segregation and euploidy. There is growing evidence of mitotic cell cycle components that are uniquely required in the germ line to ensure genome integrity. We previously showed that the primary phenotype of *germ cell deficient 2 (gcd2)* mutant mice is infertility due to germ cell depletion during embryogenesis. Here we show that the underlying mutation is a mis-sense mutation, R308K, in the motor domain of the kinesin-8 family member, KIF18A, a protein that is expressed in a variety of proliferative tissues and is a key regulator of chromosome alignment during mitosis. Despite the conservative nature of the mutation, we show that its functional consequences are equivalent to KIF18A deficiency in HeLa cells. We also show that somatic cells progress through mitosis, despite having chromosome alignment defects, while germ cells with similar chromosome alignment defects undergo mitotic arrest and apoptosis. Our data provide evidence for differential requirements for chromosome alignment in germ and somatic cells and show that Kif18a is one of a growing number of genes that are specifically required for cell cycle progression in proliferating germ cells.

Introduction

In mice, the development of germ cells begins with specification of primordial germ cells at the base of the allantois at embryonic day (E) 7.5. The newly established primordial germ cells then migrate through the dorsal mesentery and split into two laterally migrating groups that colonize the urogenital ridges between E10.5 – E12.5. During their migratory phase and

Corresponding authors: Laura G. Reinholdt, PhD, The Jackson Laboratory, 600 Main Street, Bar Harbor, ME 04609 USA, Phone: 1 (207) 288-6693, laura.reinholdt@jax.org, Jason Stumpff, PhD, Department of Molecular Physiology and Biophysics, University of Vermont, 89 Beaumont Avenue, Burlington, Vermont 05405 USA, jstumpff@uvm.edu.

during colonization of the emergent fetal gonads, primordial germ cells proliferate with an ~16h doubling time, expanding from a population of less than 100 cells to ~25,000 at E13.5 [1,2]. Further expansion of the germ cell population occurs only in the male germ line with the proliferation of spermatogonial stem cells and spermatogonia in the testes resuming just after birth and continuing through the reproductive life of the male.

While meiosis is certainly the most well-recognized cell cycle specialization occurring in the germ line, there is also evidence for mitotic cell cycle specialization. This specialization is evident in the viable, yet infertile phenotypes of mice deficient for ubiquitously expressed mitotic and DNA repair genes. Among these is *Mad2l2* (*Rev7*), a sub-unit of the translesion repair DNA polymerase zeta and a component of the spindle assembly checkpoint. *Mad2l2* is uniquely required for cell cycle regulation soon after germ cell specification when primordial germ cells are programmed to briefly arrest in G2 and undergo epigenetic reprogramming[3,4]. Similarly, the DNA repair proteins Fanconi anemia complementation group L and C (*FancL* and *FancC*), as well as minichromosome maintenance helicase 9 (*Mcm9*) are uniquely required for progression of the germ cell cycle[5-8]. However, unlike *Mad2l2*, these DNA repair genes are also required for proliferation of germ cells during colonization of the genital ridge. The peptidylprolyl cistrans isomerase gene, *Pin1*, which modulates the cell cycle by regulating cyclin E turnover is also specifically required in the developing germ line for cell cycle progression[9,10]. *Pin1*, as a catalyst for conformational changes in phosphoproteins, was later shown to have key roles in cancer, ageing and Alzheimer's disease.

We previously reported that the recessive, ethylmethanosulfonate (EMS) induced mutation, *germ cell depletion 2* (gcd2) causes infertility in mice due to germ cell depletion during embryogenesis that is first evident in E11.5 embryos during colonization of the genital ridge. In adult mutant mice, there is gonad aplasia and infertility affecting both sexes with varying severity depending on inbred strain background. Here we report that the underlying mutation is a missense mutation in *Kif18a*. *Kif18a* is a member of the kinesin-8 subfamily of motor proteins and is broadly required for control of kinetochore microtubule dynamics and chromosome alignment during mitosis[11-13]. The *Kif18a*^{gcd2} mutation results in a conservative, arginine to lysine amino acid change at a highly conserved position in the motor domain of the protein. By expressing this mutation in HeLa cells, we show that despite it's conservative nature, this mutation is sufficient to prevent the accumulation of KIF18A at the plus ends of kinetochore microtubules, leading to chromosome alignment defects and mitotic arrest. In contrast and consistent with the viable phenotype of *gcd2* mutant mice, primary somatic cells from *gcd2* mutant embryos do not arrest in mitosis despite having chromosome alignment defects and impaired growth *in vitro*. Finally, we found that germ cells (and not somatic cells) from *gcd2* mutant fetal gonads exhibit cell cycle arrest and apoptosis, ultimately leading to germ cell depletion and infertility. Thus, it appears that *Kif18a*, a key regulator of chromosome alignment, is a new member of a growing number of mitotic proteins and DNA repair factors that are ubiquitously expressed but uniquely required for germ line development. Our data also show that while KIF18A mediated chromosome alignment is dispensable in the soma, it is uniquely required for germ line development.

Materials and methods

Ethics statement

All procedures involving mice were approved by The Jackson Laboratory's Institutional Animal Care and Use Committee and performed in accordance with the National Institutes of Health guidelines for the care and use of animals in research. The strains used for this study were CAST.129S1(B6)-*gcd2*/JcsMmjax (Mouse Mutant Resource and Research Center, stock # 034325-JAX), C57BL/6J (The Jackson Laboratory stock, #000664), C57BL/6J-*Kit*$^{W\text{-}v}$/J (The Jackson Laboratory, stock #000049) and B6.Cg-*Kit*^{W}/J (The Jackson Laboratory, stock #000164)

High-throughput targeted sequencing and validation

High molecular weight, total genomic DNA was extracted from *gcd2/gcd2* spleen by phenol chloroform extraction of enriched nuclei. DNA was fragmented (Covaris), end-repaired using T4 DNA polymerase, PNK and Taq DNA polymerase (New England Biolabs) and column purified. Sequencing adapters were ligated (Roche) and the resulting fragments were size selected (300-350 bp) using agarose gel electrophoresis followed by gel extraction (Qiagen MinElute). The sample was amplified by PCR (Phusion enzyme, New England Biolabs) and then hybridized to a custom Agilent 1M feature array containing overlapping DNA probes representing the *gcd2* mapped interval (Chr2:108,786,520-109,929,176 bp (GRCm38/mm10)[14] for 65 hours according to the manufacturer's instructions (Agilent Technologies). The bar-coded, eluted samples were multiplexed with several other samples and sequenced 2 × 72 bp on an Illumina Genome Analyzer II. Approximately 6 million reads with an average read length of 68 bp were generated. A reference based (GRCm83/mm10) alignment was performed using the Burrows Wheeler Aligner (BWA) [15] and nucleotide variants were detected using SAM tools (mpileup)[16]. All resulting variants were annotated using a custom annotation tool and compared to known, strain specific SNPs from dbSNP as well as SNPs from the Sanger Mouse Genomes project [17]. Of 58 coding and/or splice site variants discovered in the data, 54 were known strain specific SNPs and 4 were novel.

HeLa cell culture, transfection, plasmids and fixation

HeLa cells were cultured in MEMα containing 10% FBS. For siRNA-mediated depletion, cells were treated with Silencer Validated siRNAs (Life Technologies) targeting Kif18A (GCUGGAUUUCAUAAGUGG) or Silencer Negative Control #1 complexed with RNAiMax (Life Technologies) following the manufacturer's instructions. An siRNA-resistant Kif18A clone was created by introducing silent mutations into the Kif18A open reading frame via PCR mutagenesis (T84A, A87C, T90C and T93C). This product was cloned into a modified EGFP-C1 vector using Gateway cloning (Life Technologies). Point mutations were introduced into the siRNA-resistant EGFP-Kif18A clone using the Quickchange II site-directed mutagenesis kit (Stratagene) to create EGFP-Kif18A-R308K (G923A) and EGFP-Kif18A-R308A (A922G and G923C). All open reading frames were confirmed by DNA sequencing. For localization studies of EGFP-Kif18A clones, HeLa cells were transfected with plasmid DNA encoding siRNA-resistant EGFP-Kif18A, EGFP-Kif18AR308K or EGFP-Kif18A-R308A 8 hours after siRNA treatment. Cells were fixed in

1% paraformaldehyde/ −20°C methanol for 10 minutes 24 hours after DNA transfection. Cells were immunofluorescently labeled with the following primary and secondary antibodies: human anti-centromere (Antibodies Inc., 2.5 ug/mL), mouse anti-gamma tubulin GTU-88 (Sigma, 0.5 ug/mL), goat anti-human Alexa Fluor 594 (Life Technologies, 2 ug/mL) and goat anti-mouse Alexa Flour 647 (Life Technologies, 2 ug/mL). Cells were imaged on an Eclipse Ti microscope (Nikon) equipped with a Clara CCD camera (Andor), Spectra X light engine (Lumencore), 100X 1.49 NA TIRF objective (Nikon) and NIS Elements software (Nikon). Optical sections were obtained every 200 nm through each mitotic spindle and maximum intensity projections of 10 optical sections at the center of each spindle are displayed. Kinetochore distributions were quantified as previously described [13,18].

Western blot analyses

HeLa cells were lysed in RIPA buffer (50 mM Tris-HCl pH 7.4, 150 mM NaCl, 2 mM EDTA, 1% NP-40 and 0.1% SDS) 20 hours after DNA transfection and 28 hours after siRNA addition. Lysates were extracted on ice for 10 minutes. An equal volume of 2X Laemmli buffer was then added and lysates were boiled for 10 minutes. Lysates were separated by electrophoresis on 4-15% Tris-glycine polyacrylamide gels (BioRad) and transferred to PVDF membrane (BioRad). Membranes were blocked in TBS (Tris-buffered saline- 50 mM Tris-Cl pH 7.4 and 150 mM NaCl) containing 5% milk. Blocked membranes were probed with 1 g/ml rabbit-anti-Kif18A antibodies (Bethyl Laboratories), 0.5 g/ml mouse-anti-GAPDH antibodies (Millipore), DyLight 800 anti-rabbit IgG and DyLight 680 anti-mouse IgG antibodies (Thermo Scientific) diluted in TBS containing 5% milk and 0.1% Tween-20. Secondary antibody fluorescence was detected with an Odyssey CLx (LI-COR).

Mouse embryonic fibroblast (MEF) derivation

Mouse embryonic fibroblasts (MEFs) were derived from E12.5-E13.5 (embryonic day 12.5-13.5) embryos. Embryos were decapitated and eviscerated in sterile, PBS (Life Technologies, Invitrogen) on ice and then moved into ~3 ml of pre-warmed (37°C) 0.05% Trypsin-EDTA (Life Technologies, Invitrogen), one embryo per well in a sterile 6 well culture dish. Each embryo was macerated with forceps and further dissociated by passing the resulting slurry through a 16-gauge needle. Following a 3 min. incubation, each tissue suspension was added to separate 15 ml conical tubes containing an equal volume of pre-warmed (37°C) MEF medium (Dulbecco's Modified Eagle Medium (DMEM, high glucose, no glutamine, no sodium pyruvate; Invitrogen) with 10% FBS (fetal bovine serum, ES grade, Lonza), 1X PenStrep (Invitrogen) and 2 mM GlutaMAX (Invitrogen)). After allowing large tissue fragments to settle, each cell suspension was transferred to a new conical tube and centrifuged at 150xg for 5 min. The resulting pellets were resuspended in 1 ml of MEF media and then added to separate 60 mm, gelatinized tissue culture plates containing 3.5 ml of MEF media. Cultures were incubated at 37°C, 5% CO_2 and were propagated by passaging 1:3 every 2-3 days. For growth curves, 9 independent MEF lines (3 +/+, 3 *Kif18a*^{gcd2}/+ and 3 *Kif18a*^{gcd2}/*Kif18a*^{gcd2} were plated in 7 triplicates (one per 24 hour point) on 12-well cell culture plates at a density of 2×10^5 cells/ml. For counting, one triplicate set of cells from each genotype was trypsinized, washed once with PBS, and counted on an

Auto-T4 Cellometer cell counter (Nexcellom). This was repeated with each triplicate every 24 hours over a period of seven days.

Live cell imaging

To maximize the number of cells in G_2/M, confluent MEF cultures were washed once with PBS and starvation medium (MEF medium without serum) was added. Cells were incubated in starvation medium at 37°C, 5% CO_2 for 48 hours. Synchronized MEFs were cultured in glass bottom dishes (MatTek) in standard MEF media and then changed to CO_2-independent media with 10% FBS (Life Technologies) for imaging. Multiple fields of cells were imaged at 2-minute intervals by Differential Interference Contrast microscopy for up to 16 hours with a 40X lens on the temperature controlled Eclipse-Ti system described above. Mitotic duration was calculated as the time from nuclear envelope breakdown to the onset of anaphase.

Mitotic profiling

Synchronized MEFs were trypsinized and plated at a density of 3×10^5 cells/ml on glass coverslips treated with 0.1% gelatin in standard MEF media containing serum. After 24 hours, cells were fixed with 4% v/v paraformaldehyde in PBS. For sequential immunolabeling, cells were washed with PBS, permeabilized and blocked with 0.1% Triton X-100 and 5% FBS respectively. Primary and secondary antibody incubations were one hour at room temperature followed by 10 min. incubation in Hoechst 33342 trihydrochloride trihydrate (Life Technologies, Molecular Probes, H1399) to counterstain DNA. Primary antibodies were anti-α tubulin (Abcam Ab18251) and anti-centromere proteins (derived from CREST patients, Antibodies Inc., 15-234) and both were used for immunofluorescence at a dilution of 1:200. Coverslips were mounted on microscope slides overnight using Vectashield hard-set mounting medium (Vector Laboratories, H-1400), and imaged on a Leica SP5 confocal microscope or a Zeiss AxioImager epifluorescence microscope.

Flow Cytometry and Terminal Deoxynucleotidyl Transferase Nick-End Labeling (TUNEL) assays

MEFs—Confluent MEFs were trypsinized, washed in PBS, fixed with ice-cold 100% v/v methanol, and stored at −20°C. To prepare cells for flow cytometry, aliquots of 1×10^6 cells/ml were washed with PBS containing 1% FBS, and blocked using BD Perm/Wash buffer (BD Bioscience) at room temperature for 15 min. All subsequent washes were also with BD Perm/Wash. MEFs were incubated for one hour at room temperature in diluted antibodies. After immunolabeling, cells were washed and then stained in a solution containing 0.1% v/v Triton X-100, 0.2mg/ml RNAse A (Life Technologies, Invitrogen), and 0.2 mg/ml propidium iodide (PI) (Life Technologies, Molecular Probes, P3566) in PBS for one hour. Cells were sorted on a FACSCalibur fluorescence-activated cell sorter (BD Biosciences), with voltage gating optimized for both Alexa Fluor-488 and propidium iodide.

To generate positive control samples, apoptosis was induced by culturing cells with 40 μM cisplatin for 16 hours. Media were collected and centrifuged for 5 minutes at 1,000 RPM to collect any non-adherent cells. Adherent cells were collected by trypsinization and added to the previously collected, non-adherent cells. Total cells were washed once with PBS, fixed

with 4% paraformaldehyde on ice for 15 minutes and washed twice with PBS. Cells were resuspended in a minimal volume of PBS, added to 5 ml ice-cold 70% ethanol and stored overnight at −20°C. Aliquots of 1×10^6 cells/ml were washed and stained using an APO-BrdU™ TUNEL Assay Kit (Life Technologies, Invitrogen, A23210) according to the manufacturers instructions. An AlexaFluor 488 conjugated primary antibody against BrdU (Life Technologies A35126, 1:20) was used for detection. Samples were processed on a FACS Calibur fluorescence-activated cell sorter with voltage gating optimized for Alexa Fluor 488. All p values were calculated using unpaired, two sample Student's t-test.

Fetal gonads—Urogenital ridges (E11.5) and fetal gonads (E12.5) with accompanying mesonephroi were dissected from E11.5 or E12.5 embryos in 1X PBS. Tissues were rinsed in 1X PBS and incubated in 1X 0.05% trypsin-EDTA (Life Technologies 25300-120) at 37°C for 15 min. Trypsin was inactivated with DMEM supplemented with 20% FBS and the suspension was pipetted through a 40μm cell strainer. Cells were washed once with PBS, fixed with 4% paraformaldehyde on ice for 15 minutes and washed twice with PBS. Cells were resuspended in a minimal volume of PBS, added to 2 ml ice-cold 70% ethanol and stored overnight at −20°C. Cells were pelleted and resuspended in diluted primary antibody ((mouse anti-phospho-histone H3 (Ser10), clone 3H10 (Millipore, 05-806, 1/500), rabbit anti-DDX4/MVH (Abcam, 13840, 1/100)) for two hours at 37°C, washed 3x, and resuspended with diluted secondary antibody in the dark for one hour at 37°C. Cells were washed and then stained in a solution containing 1% FBS, and 2 ug/ml DAPI for 30 minutes at room temperature. Cells were sorted on a LSRII Fluorescence-activated cell sorter (BD Biosciences), with voltage gating optimized for Alexa Fluor-488, Alexa Fluor-647, and DAPI. For TUNEL labeling, fixed cells were stained using an APOBrdU™ TUNEL Assay Kit (Life Technologies) according to the manufacturer's instructions using the kit controls. After the anti-BrdU incubation, cells were rinsed 2X in Perm/Wash and labeled with an antibody to mouse vasa homolog (MVH) as described above. Samples were processed on a LSRII fluorescence-activated cell sorter with voltage gating optimized for Alexa Fluor 488 and Alexa Fluor 647. All p values were calculated using unpaired, two sample Student's t-test.

RT-PCR

Tissues were dissected in PBS, immediately transferred to RNA*later* (Life Technologies) and stored at 4°C (up to 1 week) or −80°C (long term). Tissues were homogenized for 1 minute at 50 Hz using a TissueLyserLT (Qiagen) according to the manufacturer's instructions and RNA was extracted using an RNeasy Mini Kit (Qiagen). SuperScript III First Strand Synthesis System (Invitrogen) was used to generate cDNA for RT-PCR according to the manufactuer's instructions. Optimal cycle number and amount of cDNA was determined empirically for *Kif18a*. Primers and cycling conditions for *Actb* were according to the manufacturer's instructions. *Kif18a* primers flanked exons 10 – 13 with a product size of 736 bp and 0.5 l of cDNA were added to each reaction. Primer sequences are provided in Supplemental Table 1.

Whole-mount *in situ* hybridization (WISH)

RNA probes for WISH were generated from cDNA clones obtained from Open Biosystems, (*Kif18a* clone ID 3499835, *Pou5f1 (Oct3/4)* clone ID 30019896). Restriction digests were performed (EcoR1 and XhoI for *Kif18a* and EcoRI and Eba1 for *Oct3/4*) to remove the 3′ polyA and T7/Sp6 promoter sites. T7 and SP6 linkers were added and the resulting fragments used as template for *in vitro* transcription according to manufacturers instructions (DIG RNA Labeling Mix, Roche). RNA probe sequences are provided in Supplemental Table 1. Embryos were harvested at E12.5 into 1X PBS and fetal gonads were removed. Tissues were fixed in 4% paraformaldehyde (PFA) overnight followed by a dehydration series in a methanol gradient (25%, 50%, 75%, 100% in PBS with 0.1% Tween-20, PBST) 5 minutes each with shaking at room temperature. WISH was carried out as previously described with optimization for fetal gonads[1]. Specifically each pair of E12.5 fetal gonads was digested in 0.5 ml of 10 g/ml proteinase K for 9 minutes. The signal from the digoxigenin labeled probe was detected with NBT/BCIP substrate mix (Roche, #11681451001) followed by cold PBST washes, (3×5 min each) and the tissue was subsequently carried through a graded glycerol series to reduce background (25%, 50%, 80%). For imaging, fetal gonads were placed into 1X PBS and mounted on 1% agarose.

Immunohistochemistry

Testes from 6-8 dpp mice were dissected in PBS and fixed in 4% PFA overnight at 4C. Tissues were embedded in paraffin and sectioned at 5 μm thickness. Sections were deparaffinized and antigen retrieval was performed by immersing slides in 10mM sodium citrate, pH 6 and heating to 95°C for 30 min. Sections were then washed in 3 × 5 min in PBS followed by 2 × 5 min. washes with 50mM ammonium chloride. Sections were then blocked for 1 hour with PBS, 10% goat serum, 0.05% Triton X. Sections were incubated overnight at 4°C with one or more of the following antibodies, mouse anti-phospho-histone H3 (Ser10), clone 3H10 (Millipore, 05-806, 1:500), rabbit anti-DDX4/MVH (Abcam, ab 13840, 1:100), rabbit anti-MAD2 (Bethyl Laboratories, A300-301A, 1:200) and human anti-CREST used at dilution of 1:500. Sections were then washed 3 × 5 min. in PBST before addition of secondary antibodies. They were then counterstained with 0.01% Sudan Black followed by DAPI and PBS washes. Sections were mounted in 80% glycerol for imaging with Zeiss AxioImager.Z2.

Results

Mice homozygous for the EMS (ethylmethanesulfonate) induced mutation, *gcd2 (germ cell depletion 2)* are infertile due to depletion of post-migratory germ cells at embryonic day (E) 11.5. Previously, we mapped the mutation to an ~1 Mb region on Chromosome 2 between 108,786,520-109,929,176 bp (GRCm38/mm10) containing 6 protein coding genes, including *Mettl15, Kif18A, Bdnf, Lin7c, Gm18939* and *Lgr4*[14].

To identify the underlying causative mutation, we used high-throughput, targeted sequencing of the entire 1.1 Mb interval on chromosome 2 (Chr2: 108,786,520-109,929,176)[19] and generated ~2M 76 bp, paired end reads from an affected *gcd2/gcd2* individual. When mapped to the reference genome, these data resulted in 85X

median coverage across 97% of the target interval, including all coding sequence, introns, and conserved non-coding sequence and excluding 3% repetitive sequence. From the resulting alignment, a total of four novel variants were called and all were subsequently validated by Sanger sequencing of additional mutant, heterozygous and wild type samples from the *gcd2* colony, as well as CJ7 (129/SvImJ) ES cells, representing the genome in which the *gcd2* mutation was originally induced[20]. Of these 4 variants, 2 were heterozygous in the sequenced *gcd2/gcd2* sample and could not be validated by subsequent capillary sequencing. These were deemed sequencing or alignment artifacts. The third variant (Chr2: 109,908,059 G to T, GRCm38, mm10) was found in *gcd2* samples, but was also found in the wild type, parental CJ7 ES cell line, as well as in DNA from the 129/SvImJ inbred strain. The fourth variant (Chr2: 109,296,645 (GRCm38, mm10), G to A in exon 7 of *Kif18a*) was found only in *gcd2* samples with 100% concordance to sample genotypes. Subsequent typing of the *gcd2* colony showed perfect linkage between this missense mutation and the phenotype (N~895), moreover allele specific PCR genotyping for this mutation was used to create two congenic lines (>N9) both of which retain the original phenotype after over 9 generations of backcrossing and selection for the mutation. Finally, consistent with the guanine alkylation activity of EMS, the *gcd2* mutation is a G to A transition. The predicted consequence of this mutation is a single, conservative amino acid change, R308K, occurring in a highly conserved amino acid within the kinesin motor domain (Fig. 1).

KIF18A is a microtubule attenuating kinesin motor that accumulates at the fast growing, plus ends of microtubules where it functions to regulate microtubule dynamics[21,22]. During mitosis, this activity is required to restrict mitotic chromosome oscillations to the equator of the mitotic spindle during metaphase[13]. Studies of kinesin-1 motors indicate that the conserved arginine residue mutated in *Kif18a*^{gcd2} mice directly contacts beta-tubulin and is required for binding of kinesin to microtubules [23,24]. Mutation of the equivalent arginine residue in human kinesin-1 to alanine (R278A) reduces the microtubule-stimulated ATPase activity of the motor by more than 15-fold[23]. To determine the consequences of mutating R308 on KIF18A function during mitosis, we expressed wild type KIF18A, KIF18A-R308K or KIF18A-R308A fused with EGFP in HeLa cells depleted of endogenous KIF18A (Fig. 2A). Unlike the wild type protein, the mutant proteins did not accumulate at kinetochore microtubule plus ends and instead remained distributed along the length of the kinetochore microtubules (Fig. 2B). Moreover, HeLa cells expressing the mutant protein exhibited a significant increase in the distribution of kinetochores within the spindle (Fig 2. C-E), similar to that seen in cells depleted of wild type KIF18A[13]. Taken together, these data indicate that R308 is required for KIF18A's chromosome alignment function.

To investigate the consequences of the *Kif18a*^{gcd2} mutation in primary cells we derived mouse embryonic fibroblasts (MEFs) from mutant and littermate control E12.5-E13.5 embryos. Mutant MEFs grew slowly in culture (Fig. 3A) and had lower viability by dye exclusion (Fig. 3B). Since KIF18A-depleted HeLa cells arrest in mitosis, we surmised that the slow growth of mutant MEFs might be due to mitotic arrest. However, cell cycle analysis based on DNA content and labeling with phosphorylated histone H3 (a marker of late G2/M phase), revealed that unlike *Kif18a*^{R308K} expressing HeLa cells, mutant MEFs did not show evidence of mitotic arrest or increased apoptosis (Fig. 3C-E). To confirm that

Kif18a^{gcd2} MEFs do not arrest in mitosis, we imaged live dividing cells via differential interference contrast microscopy (DIC). These studies revealed that wild type and *Kif18a*^{gcd2} MEFs progress from nuclear envelope breakdown to anaphase with comparable timing (Figure 4A-B).

In KIF18A depleted HeLa cells, impaired mitotic chromosome alignment is associated with activation of the spindle assembly checkpoint, mitotic arrest and apoptosis[25]. Based on these data, we surmised that mutant *Kif18a*^{gcd2} MEFs progress through mitosis with normal chromosome alignment. To test this, we assessed chromosome distribution in mutant and wild type MEFs during mitosis. Surprisingly, mutant MEFs displayed a 7-fold increase in the ratio of preanaphase mitotic cells with unaligned versus aligned chromosomes (Fig. 5A-B). Consistent with these data, we also observed that chromosomes were not aligned in live *Kif18a*^{gcd2} MEFs prior to anaphase (Fig. 4A-B).

The mitotic phenotype of *Kif18a*^{gcd2} mutant MEFs notwithstanding, *Kif18a*^{gcd2} mutant mice are viable with respect to their wild type littermates. Both *Kif18a*^{gcd2} and *Kif18a*$^{-/-}$ animals are otherwise overtly normal with the exception of infertility due to germ cell depletion[14,26]. It should be noted that while infertility is seen in both sexes of *Kif18a*^{gcd2} mice, male specific infertility and gonad aplasia was reported for *Kif18a*$^{-/-}$ mice and in these studies infertility was not attributed to germ cell depletion during embryogenesis [26]. We also previously showed that germ cell depletion in *Kif18a*^{gcd2} mutant mice is highly sensitive to strain background[14], which might underlie the male specific infertility that was previously reported for *Kif18a*$^{-/-}$ mice. The germ cell specific phenotype suggests that *Kif18a* is specifically expressed in the germ line and/or its expression is tightly regulated in the germ line. Data published by Liu *et al*. show that *Kif18a* RNA and protein are found in a variety of adult tissues in addition to the adult ovary and testes[26], and is particularly abundant in proliferative tissues. To expand this expression analysis to the developmental time point where functional *Kif18a* is required for fertility, we used and *in situ* hybridization to examine expression in E11.5-12.5 fetal gonads[14]. As expected, we found that *Kif18a* is expressed in the fetal gonad at E11.5-12.5 and by comparing the expression pattern of *Kif18a* to a germ cell specific gene, *Pou5f1* (*Oct3/4*), we found that *Kif18a* does not exhibit a germ cell specific expression pattern (Fig. 6A). Using RT-PCR we found that *Kif18a* is expressed in both wild type and *Kif18a*^{gcd2} mutant fetal gonads. Qualitatively, *Kif18a* expression was highest in the adult testes, which has the largest population of proliferating germ cells (Fig. 6B, lane 8). In contrast, *Kif18* expression was lowest in *Kif18a*^{gcd2} and *Kit*$^{W/W\text{-}v}$ adult mutant ovaries and testes, which are devoid of proliferating germ cells (Fig. 6B, lanes 6, 7, 10). *Kif18a* expression is still detectable in the absence of proliferating germ cells, lending further support to the conclusion that *Kif18a* expression in the gonad is not restricted to the germ line. Unfortunately, commercially available KIF18A antibodies did not provide specific labeling in fetal gonads so the *in-situ* data could not be correlated with protein localization.

To determine the consequences of the *Kif18a*^{gcd2} mutation on mitotic progression in germ cells, we performed cell cycle analysis on E12.5 fetal gonads, using an antibody to the germ cell specific mouse VASA homolog MVH/DDX4 to distinguish between germ cells (MVH positive) and somatic cells (MVH negative). There were more *Kif18a*^{gcd2} mutant germ cells

in G2/M when compared to germ cells from wild type littermate controls (Fig. 7A). There was also a corresponding reduction in the percentage of mutant germ cells in G1. A significantly higher percentage of *Kif18a*^{gcd2} mutant germ cells were positive for phosphorylated histone H3 and TUNEL (Fig. 7B-C). Importantly, there were no significant differences in cell cycle distribution or histone H3 phosphorylation in gonadal somatic cells (MVH negative) from mutant and wild type animals (Fig. 7B). Taken together these data provide evidence that mutant germ cells in the E12.5 fetal gonad exhibit mitotic arrest, which may ultimately lead to germ cell depletion and infertility. Since mutant gonads are not completely devoid of germ cells at birth[14], mitotic arrest appears to affect a specific population of germ cells.

To determine if *Kif18a*^{gcd2} mutant germ cells have underlying chromosome alignment defects, we used immunohistochemistry with antibodies recognizing alpha tubulin and the germ cell specific, GCNA (germ cell nuclear antigen) to examine mitotically dividing germ cells (spermatogonia) from testes at 6 days post partum. Aberrant spindle organization and defects in chromosome alignment were apparent in GCNA positive spermatogonial cells from pre-pubertal mutant testes (Fig. 7D). To determine if persistent unattached kinetochores underlie activation of the spindle checkpoint, we immunolabeled with an antibody against the checkpoint protein MAD2. MAD2 localization to kinetochores provides a signal that inhibits progression from metaphase to anaphase[27,28]. We found that MAD2 is associated with kinetochores regardless of their position within the spindle in all (100%, N=40) mutant spermatogonia whereas MAD2 co-localization with kinetochores was more rare (30%, N=40) and more frequently associated with kinetochores of chromosomes off of the metaphase plate in wild type spermatogonia (Supplementary Figure 1). These data, combined with the observed increase in the fraction of mitotic germ cells within *gcd2* embryos, are consistent with loss of KIF18A function leading to a germ cell specific mitotic arrest due to kinetochore-microtubule attachment defects.

Discussion

We found that the causative mutation underlying *gcd2* is a G to A (Chr2: 109,296,645 (GRCm38, mm10)) transition in exon 7 of *Kif18a*; a mutation that results in a conservative amino acid change, R308K, in the motor domain of the protein. Recent crystal structure data show that the homologous arginine in the motor domain of kinesin-1 is a key residue in contact with β-tubulin when the motor is bound to microtubules [24]. Therefore, despite having similar properties (positively charged and polar), lysine is likely a poor functional substitute for arginine at this position. Consistent with this, expression of KIF18A-R308K in HeLa cells was functionally equivalent to KIF18A knockdown and to the more severe amino acid change, R308A, providing further evidence that this mis-sense mutation is a functionally null allele. Finally, the primary infertility phenotype of knockout *Kif18a* mice is nearly identical to the phenotype of *gcd2* mice[14,26] with the exception that both male and female *gcd2* mutant mice are infertile, while only male infertility was reported in *Kif18a* knockout mice. Our previous data suggest that these differences are more likely due to differences in strain background rather than functional differences in the mutations per se (knockout allele vs. missense mutation)[14].

Unlike KIF18A-R308K expressing HeLa cells, mutant MEFs do not show evidence of G2 to M arrest or increased apoptosis, despite having chromosome alignment defects, impaired growth and reduced viability. Moreover, progression through nuclear envelope breakdown to anaphase is comparable to wild type. Therefore, the impaired growth of mutant MEFs cannot be explained by delayed cell division. Impaired growth and reduced viability in the absence of spindle checkpoint activation and apoptosis could be due to the activation of alternative programmed cell death mechanisms like autophagy or necrosis; however additional work is necessary to decipher the mitotic consequences of KIF18A deficiency in primary MEFs. Certainly, the lack of spindle checkpoint activation in primary MEFs likely explains the viability of *Kif18a*^{gcd2} mutant embryos[14] and the viability of *Kif18a* null embryos [26]. However, we previously reported that homozygous, mutant *Kif18a*^{gcd2} mice are found in slightly reduced Mendelian ratios (~13-18% depending on the genetic background) at wean. Therefore, the mitotic phenotype of mutant MEFs may well have a subtle impact on the development of mutant embryos or survival prior to weaning (3 weeks). In adult mutant animals, the relatively subtle mitotic phenotype of somatic cells could sensitize or predispose proliferative tissues to environmental or genetic cell cycle perturbations. For example, loss of KIF18A function impairs tumorigenesis in induced colon cancer mouse models [29].

While *Kif18a* expression is not restricted to the germ cells, our data show that it is specifically required for chromosome alignment and mitotic progression in the germ cell lineage. Unlike somatic cells, mutant germ cells undergo mitotic arrest and apoptosis in the absence of functional KIF18A. These events are detectable as early as 11.5 dpc in the fetal gonad, but since mutant animals are born with a small germ cell population, these events are seemingly stochastic. We examined MAD2 localization in spermatogonia from pre-pubertal testes and found persistent MAD2 localization to mutant kinetochores at metaphase, which is generally considered to be a marker of active spindle assembly checkpoint signaling due to kinetochore-microtubule attachment defects[27,28,30,31]. Thus, these data are consistent with reduced kinetochore-microtubule attachment in germ cells lacking Kif18A function. However, more in depth profiling of other checkpoint proteins and directed studies of kinetochore function in isolated spermatogonia will be required to fully understand the underlying mechanism and timing of checkpoint activation in mutant spermatogonia and why Kif18A is required for mitotic progression in germ but not somatic cells.

Previous studies have demonstrated a similar germ cell specific sensitivity to mutations that disrupt the phospho-regulation of the enzyme separase, which cleaves the cohesin complexes linking sister chromosomes at the metaphase to anaphase transition[32]. Thus, somatic and germ cells appear to either have different thresholds for mitotic progression control or somatic cells possess mechanisms that impart functional redundancy in the absence of these mitotic regulators. Regardless, our data support the notion that regulation of the mitotic spindle is different in germline and somatic cells. This is consistent with the underappreciated concept of differential cell cycle regulation in germ and somatic cells. The infertility phenotype of mice deficient for peptidylprolyl cis-trans isomerase gene (*Pin1)* provides additional support for this concept. PIN1 is required for cyclin E turnover and PIN1 deficiency leads to germ cell deficiency due to a protracted cell cycle [10,33]. Additional roles

for PIN1 in ageing, cancer, neurodegeneration, and bone density were later revealed by more extensive, specialized phenotyping of mutant mice; suggesting that additional roles for KIF18A may also exist outside the developing germ line but may require more specialized phenotyping in the context of additional environmental and/or genetic insults.

An alternative explanation for the germ cell specific cell cycle arrest observed in KIF18A deficient mice could be that KIF18A is required for aspects of germ cell development that are unrelated to chromosome alignment. Mammalian *Kif18a* was originally cloned from bone marrow stromal cells, where it was shown to associate with estrogen receptor (ER) alpha, implicating an expanded role for this kinesin in ER signaling [34,35]. A downstream consequence of ER signaling is phosphorylation of AKT and KIF18A depleted cell lines and somatic tissues are deficient in the phosphorylated form of AKT [36]. During germ line development, ER signaling is required for expression of KITL in supporting somatic cells, ultimately leading to the phosphorylation of AKT kinase in the KIT expressing germ cells which in turn promotes germ cell survival. The balance of AKT phosphorylation in the developing germ line appears to be critical for regulated proliferation of germ cells and for inhibition of germ cell tumor formation via downstream activation of p53[37]. Whether AKT phosphorylation and/or signaling is disrupted during the development of germ cells in KIF18A deficient mice remains to be seen. However, supporting the notion of an additional role outside the developing germ line, our data indicate that *Kif18A* is not specifically expressed in germ cells during fetal gonad development. Therefore, future work will be focused on conditional ablation of KIF18A function in the germ line and in the gonadal somatic cells as well as analysis of AKT signaling during germ line development in the absence of KIF18A. Since the consequences of mitotic error in germ cells can span generations, mitotic cell cycle specialization is likely the result of strong positive selection for genome integrity in the developing germ line.

Supplementary Material

Refer to Web version on PubMed Central for supplementary material.

Acknowledgements

We are grateful to the Genome Technologies service core at the Jackson Laboratory for providing high throughput sequencing and Sanger sequencing support. This work was supported by NICHD HD078485-01 to L.G.R., and a Cancer Center Core Grant CA34196 to The Jackson Laboratory. This work was also supported in part by a Basil O'Connor Research Starter Scholar Award (#5-FY14-33) and a Vermont Cancer Center/ LCCRO Program Award to J.S.

References

1. Wilkinson, DG. In Situ Hybridization: A Practical Approach. Vol. 224. Oxford University Press; USA: 1992.
2. Tam PP, Snow MH. Proliferation and migration of primordial germ cells during compensatory growth in mouse embryos. Journal of embryology and experimental morphology. 1981; 64:133–47. [PubMed: 7310300]
3. Pirouz M, Pilarski S, Kessel M. A critical function of Mad2l2 in primordial germ cell development of mice. PLoS genetics. 2013; 9:e1003712. [PubMed: 24009519]

4. Watanabe N, et al. The REV7 subunit of DNA polymerase zeta is essential for primordial germ cell maintenance in the mouse. The Journal of biological chemistry. 2013; 288:10459–71. [PubMed: 23463509]
5. Hartford SA, et al. Minichromosome maintenance helicase paralog MCM9 is dispensible for DNA replication but functions in germ-line stem cells and tumor suppression. Proceedings of the National Academy of Sciences of the United States of America. 2011; 108:17702–7. [PubMed: 21987787]
6. Nadler JJ, Braun RE. Fanconi anemia complementation group C is required for proliferation of murine primordial germ cells. Genesis. 2000; 27:117–23. [PubMed: 10951504]
7. Lu B, Bishop CE. Late onset of spermatogenesis and gain of fertility in POG-deficient mice indicate that POG is not necessary for the proliferation of spermatogonia. Biology of reproduction. 2003; 69:161–8. [PubMed: 12606378]
8. Agoulnik AI, et al. A novel gene, Pog, is necessary for primordial germ cell proliferation in the mouse and underlies the germ cell deficient mutation, gcd. Human molecular genetics. 2002; 11:3047–53. [PubMed: 12417526]
9. Yeh ES, Means AR. PIN1, the cell cycle and cancer. Nature reviews. Cancer. 2007; 7:381–8. [PubMed: 17410202]
10. Yeh ES, Lew BO, Means AR. The loss of PIN1 deregulates cyclin E and sensitizes mouse embryo fibroblasts to genomic instability. The Journal of biological chemistry. 2006; 281:241–51. [PubMed: 16223725]
11. Mayr MI, et al. The human kinesin Kif18A is a motile microtubule depolymerase essential for chromosome congression. Curr Biol. 2007; 17:488–98. [PubMed: 17346968]
12. Zhu C, et al. Functional analysis of human microtubule-based motor proteins, the kinesins and dyneins, in mitosis/cytokinesis using RNA interference. Mol Biol Cell. 2005; 16:3187–99. [PubMed: 15843429]
13. Stumpff J, von Dassow G, Wagenbach M, Asbury C, Wordeman L. The kinesin-8 motor Kif18A suppresses kinetochore movements to control mitotic chromosome alignment. Developmental cell. 2008; 14:252–62. [PubMed: 18267093]
14. Reinholdt LG, Munroe RJ, Kamdar S, Schimenti JC. The mouse gcd2 mutation causes primordial germ cell depletion. Mechanisms of development. 2006; 123:559–69. [PubMed: 16822657]
15. Li H, Durbin R. Fast and accurate long-read alignment with Burrows-Wheeler transform. Bioinformatics. 2010; 26:589–95. [PubMed: 20080505]
16. Li H, et al. The Sequence Alignment/Map format and SAMtools. Bioinformatics. 2009; 25:2078–9. [PubMed: 19505943]
17. Keane TM, et al. Mouse genomic variation and its effect on phenotypes and gene regulation. Nature. 2011; 477:289–94. [PubMed: 21921910]
18. Stumpff J, Wagenbach M, Franck A, Asbury CL, Wordeman L. Kif18A and chromokinesins confine centromere movements via microtubule growth suppression and spatial control of kinetochore tension. Developmental cell. 2012; 22:1017–29. [PubMed: 22595673]
19. D'Ascenzo M, et al. Mutation discovery in the mouse using genetically guided array capture and resequencing. Mamm Genome. 2009; 20:424–36. [PubMed: 19629596]
20. Munroe RJ, et al. Mouse mutants from chemically mutagenized embryonic stem cells. Nature genetics. 2000; 24:318–21. [PubMed: 10700192]
21. Stumpff J, et al. A tethering mechanism controls the processivity and kinetochore-microtubule plus-end enrichment of the kinesin-8 Kif18A. Mol Cell. 2011; 43:764–75. [PubMed: 21884977]
22. Du Y, English CA, Ohi R. The kinesin-8 Kif18A dampens microtubule plus-end dynamics. Curr Biol. 2010; 20:374–80. [PubMed: 20153196]
23. Woehlke G, et al. Microtubule interaction site of the kinesin motor. Cell. 1997; 90:207–16. [PubMed: 9244295]
24. Gigant B, et al. Structure of a kinesin-tubulin complex and implications for kinesin motility. Nature structural & molecular biology. 2013; 20:1001–7.
25. Mayr MI, et al. The human kinesin Kif18A is a motile microtubule depolymerase essential for chromosome congression. Current biology : CB. 2007; 17:488–98. [PubMed: 17346968]

26. Liu XS, et al. Germinal Cell Aplasia in Kif18a Mutant Male Mice Due to Impaired Chromosome Congression and Dysregulated BubR1 and CENP-E. Genes & cancer. 2010; 1:26–39. [PubMed: 20981276]
27. Chen RH, Waters JC, Salmon ED, Murray AW. Association of spindle assembly checkpoint component XMAD2 with unattached kinetochores. Science. 1996; 274:242–6. [PubMed: 8824188]
28. Li Y, Benezra R. Identification of a human mitotic checkpoint gene: hsMAD2. Science. 1996; 274:246–8. [PubMed: 8824189]
29. Zhu H, et al. Targeted deletion of Kif18a protects from colitis-associated colorectal (CAC) tumors in mice through impairing Akt phosphorylation. Biochem Biophys Res Commun. 2013; 438:97–102. [PubMed: 23872115]
30. Waters JC, et al. Mad2 binding by phosphorylated kinetochores links error detection and checkpoint action in mitosis. Curr Biol. 1999; 9:649–52. [PubMed: 10375530]
31. Waters JC, Chen RH, Murray AW, Salmon ED. Localization of Mad2 to kinetochores depends on microtubule attachment, not tension. J Cell Biol. 1998; 141:1181–91. [PubMed: 9606210]
32. Xu J, et al. Separase phosphosite mutation leads to genome instability and primordial germ cell depletion during oogenesis. PLoS One. 2011; 6:e18763. [PubMed: 21494564]
33. Atchison FW, Capel B, Means AR. Pin1 regulates the timing of mammalian primordial germ cell proliferation. Development. 2003; 130:3579–86. [PubMed: 12810604]
34. Luboshits G, Benayahu D. MS-KIF18A, a kinesin, is associated with estrogen receptor. Journal of cellular biochemistry. 2007; 100:693–702. [PubMed: 17006958]
35. Zusev M, Benayahu D. The regulation of MS-KIF18A expression and cross talk with estrogen receptor. PloS one. 2009; 4:e6407. [PubMed: 19636373]
36. Nagahara M, et al. Kinesin 18A expression: clinical relevance to colorectal cancer progression. International journal of cancer. Journal international du cancer. 2011; 129:2543–52. [PubMed: 21213216]
37. Ewen KA, Koopman P. Mouse germ cell development: from specification to sex determination. Molecular and cellular endocrinology. 2010; 323:76–93. [PubMed: 20036311]

Highlight

- *Germ cell depletion 2* is a missense mutation in the motor domain of *Kif18a*.
- *Kif18a*^{gcd2} causes chromosome alignment defects in somatic and germ cells.
- *Kif18a*^{gcd2} leads to a germ cell specific, checkpoint-mediated mitotic arrest.
- Mitotic arrest of *Kif18a*^{gcd2} germ cells causes germ cell depletion and infertility.

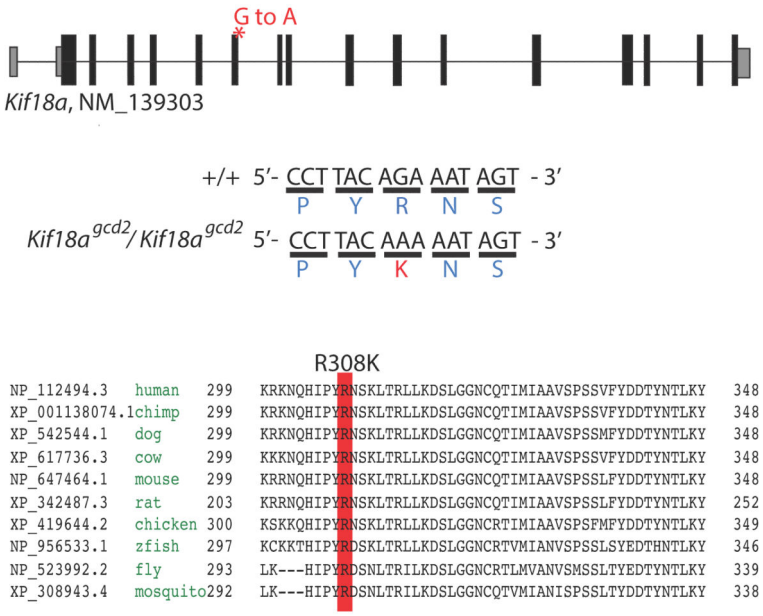

Figure 1. The *gcd2* mutation affects the highly conserved R308 residue within the KIF18A motor domain

Gcd2 is a G to A transition in exon 7 of *Kif18a*. This is a missense mutation that changes an AGA codon to an AAA, leading to the single amino acid change, R308K. Arginine 308 is a highly conserved amino acid in the motor domain of the protein.

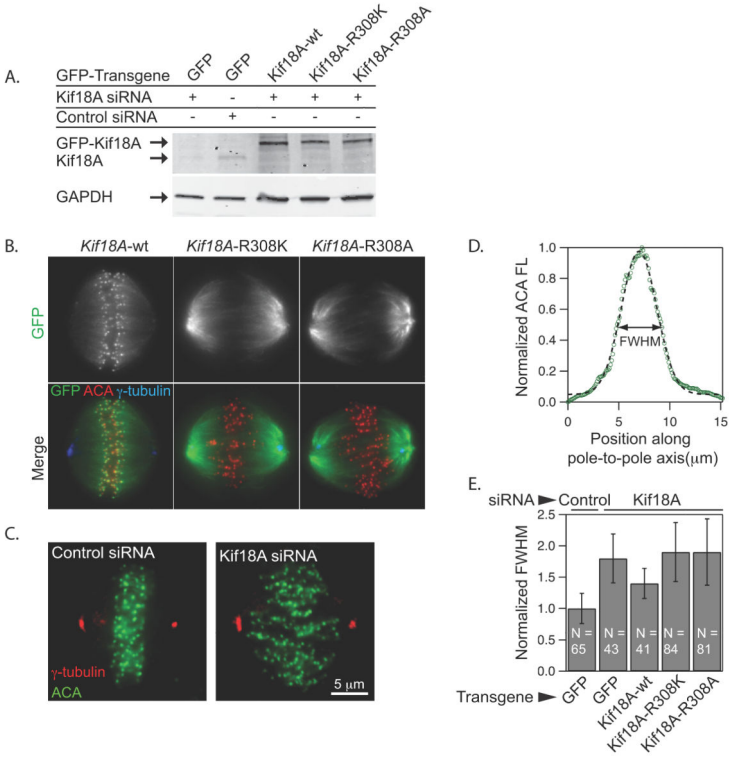

Figure 2. Mutations in R308 disrupt KIF18A's localization and chromosome alignment function

HeLa cells were treated with siRNA oligonucleotides targeting endogenous KIF18A. Cells were rescued with GFP labeled wild type KIF18A or with the mutant GFP labeled KIF18A-R308K or KIF18A-R308A (A). Unlike $KIF18A^{WT\text{-}GFP}$, $KIF18A^{R308K\text{-}GFP}$ and $KIF18A^{R308A\text{-}GFP}$ (green) failed to concentrate near kinetochores (red) and instead were distributed along the spindle between the centrosomes (γ-tubulin, blue) in KIF18A-depleted HeLa cells (B). To measure centromere alignment, the distribution of anti-centromere antigen fluorescence (ACA FL) along the normalized pole-to-pole axis was measured and the full width at half maximum (FWHM) was calculated for each condition. Representative images of control and Kif18A siRNA treated cells stained for γ-tubulin (red) and ACA (green) are shown (C). A plot of average ACA FL distribution (green circles) within a control cell is well fit by a single Gaussian function (dashed line) (D). Average FWHM measurements from HeLa cells treated with control or KIF18A siRNAs and expressing GFP or the indicated Kif18A constructs are plotted. Cells expressing KIF18A-R308 mutations displayed a similar increase in kinetochore distribution ($p > 0.05$), which were both significantly different from Kif18A-wt expressing cells ($p < 0.001$). The number of cells analyzed (N) is reported and error bars indicate SEM (E).

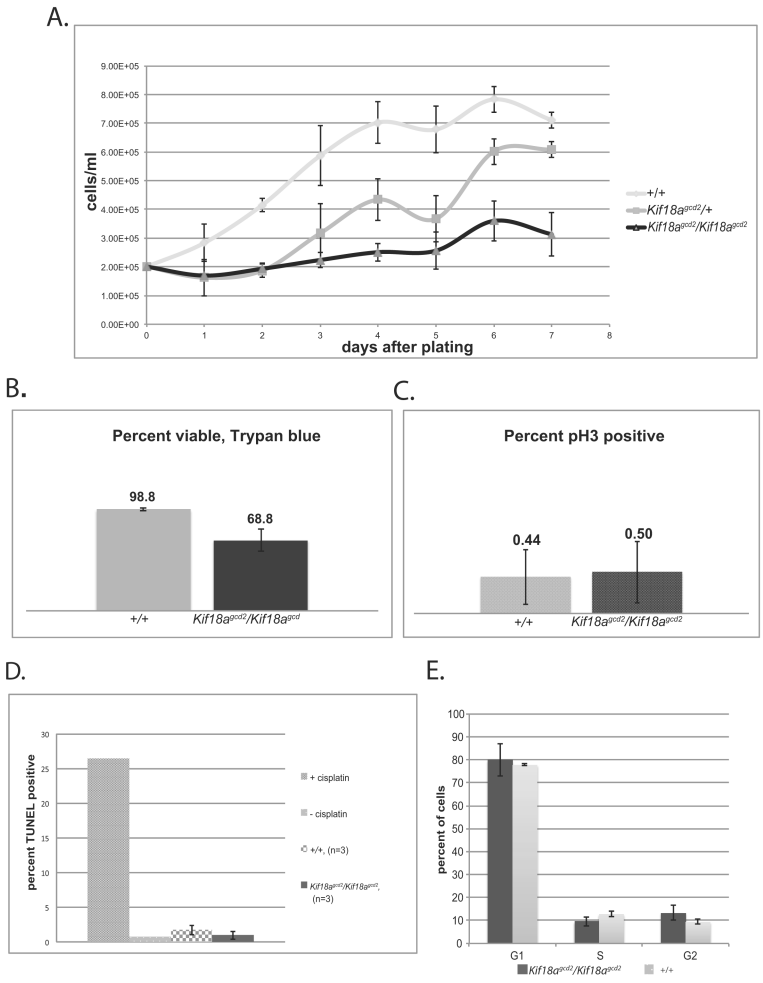

Figure 3. Primary *Kif18a*^{gcd2} embryonic fibroblasts do not display a cell cycle delay

MEFs derived from mutant embryos were slow growing (A) and had reduced viability by trypan blue exclusion (B). There were no significant differences in histone H3 ser10 phosphorylation (C), in apoptosis related DNA fragmentation (TUNEL) (D) or cell cycle staging by DNA content between mutant and wild type MEFs. All experiments were performed with three independently derived primary cell lines per genotype and technical replicates as described in the Methods.

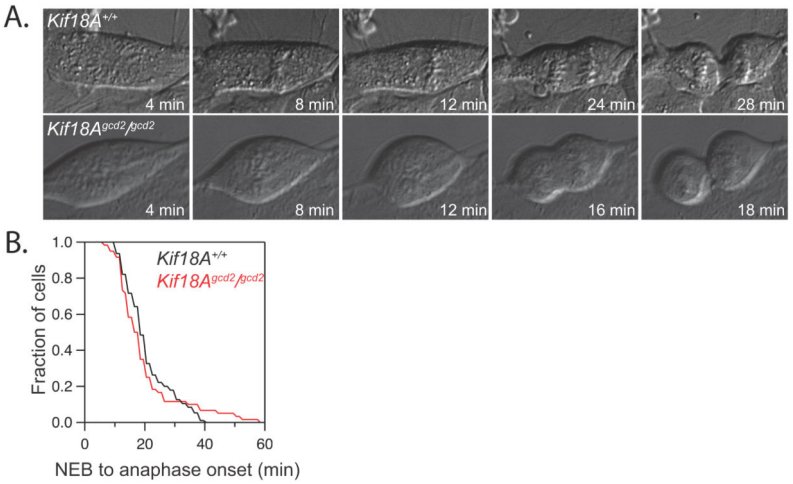

Figure 4. *Kif18a*^{gcd2} mutant and wild type MEFs progress through mitosis with similar timing

Mutant and control MEFs were imaged over a 16h period by differential interference contrast (A). Time from nuclear envelope breakdown to anaphase was recorded at 2-minute intervals and no significant difference was found between mutant and wild type MEFs ($p = 0.56$), n = 93 cells for *Kif18a*$^{+/+}$ and 58 cells for *Kif18a*$^{gcd2/gcd2}$ from 2 cell lines per genotype (B).

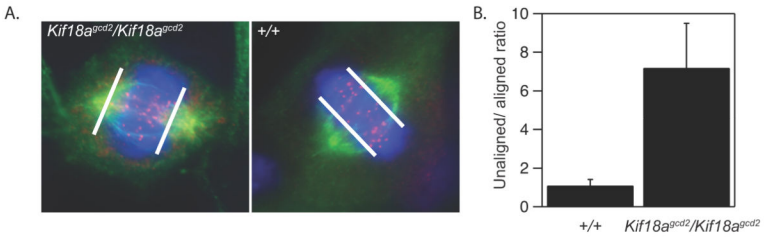

Figure 5. *Kif18a*^{gcd2} mutant MEFs exhibit chromosome alignment defects

Mitotic profiling of *Kif18a*^{gcd2} mutant MEFs immunolabeled for tubulin (green) and CREST (red, centromeres) (A) revealed a high ratio of preanaphase mitotic cells with unaligned versus aligned chromosomes in mutant MEFs compared to wild type controls, n=3 cell lines per genotype, mean +/− s.d. is displayed (B).

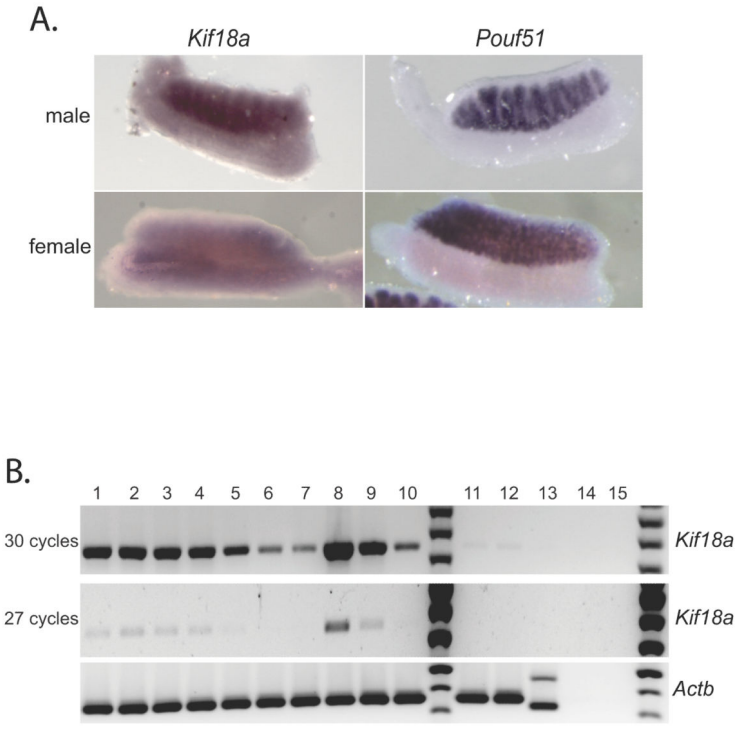

Figure 6. *Kif18a* is ubiquitously expressed in the fetal gonad

In situ hybridization of *Kif18a* and the germ cell specific *Pou5f1* (*Oct3/4*) in wild type E12.5 ovaries and testes shows that *Kif18a* expression is not restricted to the germ line (A). RT-PCR shows that *Kif18a* is expressed in the fetal gonad, as well as the adult testes and ovary. *Kif18a* expression positively correlates with the presence of proliferating germ cells (high in the wild type testes and reduced in the germ cell deficient $Kit^{W/W\text{-}v}$ testes and ovaries). Lane 1, $Kif18a^{gcd2}/Kif18a^{gcd2}$ E11.5-12.5 fetal gonad; Lane 2, +/+ E11.5-12.5 fetal gonad; Lane 3, Kit+/+ E11.5-12.5 fetal gonad; Lane 4, $Kit^{W/W\text{-}v}$ E11.5-E12.5 fetal gonad; Lane 5, C57BL/6J adult ovary; Lane 6, $Kif18a^{gcd2}/Kif18a^{gcd2}$ adult ovary; Lane 7, $Kit^{W/W\text{-}v}$ adult ovary; Lane 8, C57BL/6J adult testes; Lane 9, $Kif18a^{gcd2}/Kif18a^{gcd2}$ adult testes; Lane 10, $Kit^{W/W\text{-}v}$ adult testes; Lane 11, C57BL/6J adult liver; Lane 12, C57BL/6J adult brain; Lane 13, DNA, no RNA, no reverse transcriptase; Lane 14, no reverse transcriptase; Lane 15, PCR water control, 100 bp ladder (B).

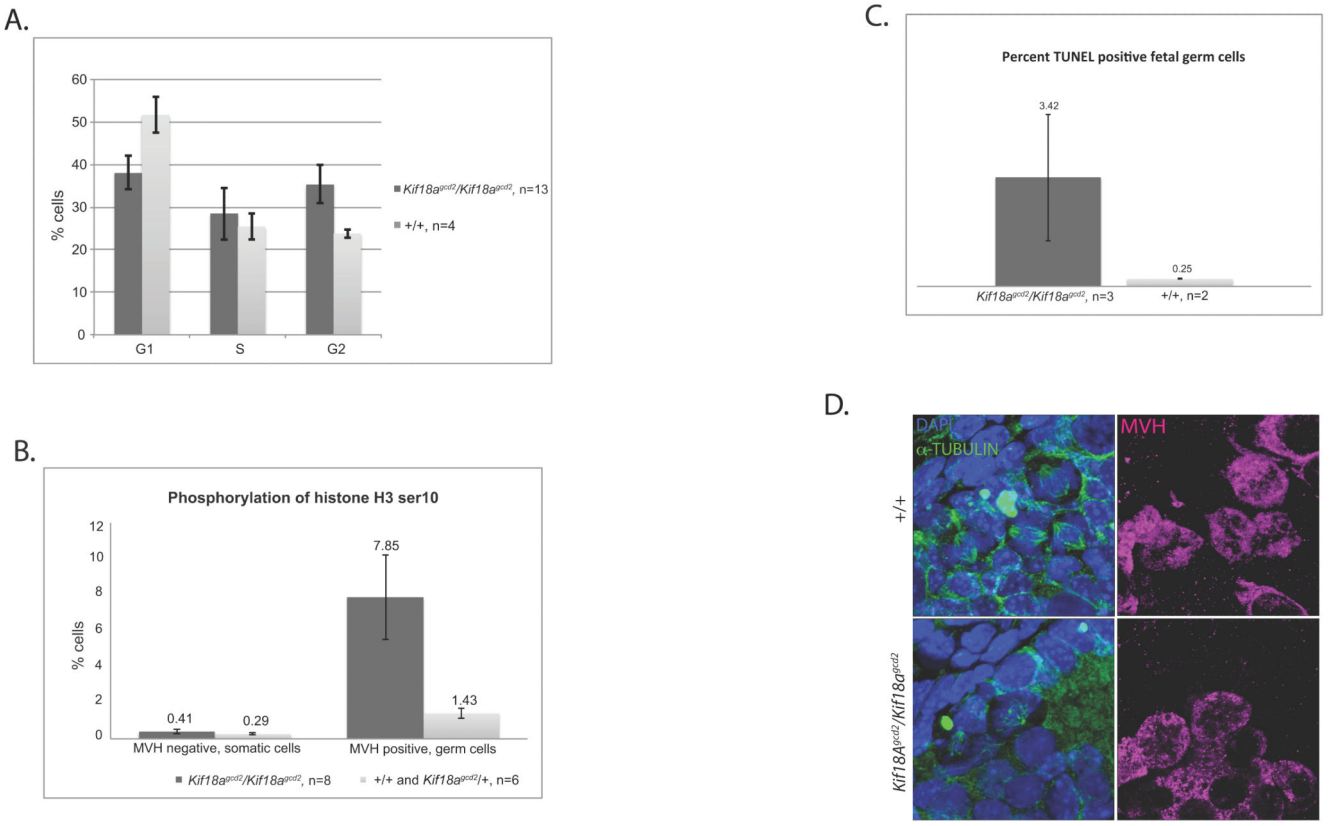

Figure 7. *Kif18a*^{gcd2} mutant germ cells arrest in mitosis with chromosome alignment defects

Cell cycle analysis by DNA content revealed a significantly higher percentage of *Kif18a*^{gcd2} mutant germ cells in G2 compared to wild type (Student's t-test, p=0.006) and a correspondingly decreased percentage of cells in G1 (Student's t-test, p=0.002) (A). Phosphorylated histone H3 (B), and TUNEL labeling (C), both indicative of G2/M checkpoint activation were significantly increased in mutant germ cells (Student's t-test (pH3, germ cells), p=0.005; Student's t-test (pH3, somatic cells), p=0.02; Student's t-test (TUNEL, germ cells), p=0.05). In all cases, error bars represent standard deviation from the mean value from at least 3 age-matched, sibling biological replicates per genotype from multiple litters. For mutant genotypes, more biological replicates were required to obtain sufficient germ cells numbers for flow cytometry. Mitotically dividing spermatogonial cells (MVH positive) from pre-pubertal, mutant testes had poor spindle organization and showed defects in mitotic chromosome alignment (D).